MNRAS 000, 1–?? (2018) Preprint 24 June 2018 Compiled using MNRAS LaTeX style file v3.0

Hercules-Aquila and Virgo Clouds with Gaia DR2. Evidence for a common origin

Keith T. Smith,[1★] A. N. Other,[2] Third Author[2,3] and Fourth Author[3]
[1] *Royal Astronomical Society, Burlington House, Piccadilly, London W1J 0BQ, UK*
[2] *Department, Institution, Street Address, City Postal Code, Country*
[3] *Another Department, Different Institution, Street Address, City Postal Code, Country*

Accepted XXX. Received YYY; in original form ZZZ

ABSTRACT
200 words for Letters. No references should appear in the abstract.

Key words: keyword1 – keyword2 – keyword3

1 INTRODUCTION

How do you hide the evidence for a massive impact event that caused the extinction of most of the dinosaurs as well as 75% of all species on Earth? You bury it deep under the sea, covered with a layer of sediment taller than the Empire State Building (?). Without the discovery of the giant Chicxulub crater, the meteorite impact hypothesis would remain a neat theory supported by striking but indirect evidence. A hypothesis of an ancient dramatic collision between the Milky Way and an unidentified massive dwarf galaxy was put forward by ? to explain a particular feature in the overall stellar halo density profile (??). Most recently, through a study of a portion of the nearby stellar halo, ? demonstrated that the great impactor must have collided with the young Milky Way on a nearly radial orbit, thus swamping the inner stellar halo with metal-rich material with orbital anisotropy (see ?) close to unity. Merger events like this tend to leave behind a battery of debris clouds and shells (see ??), which - akin to the peak rings of impact craters (see e.g. ?) - if discovered could help to reconstruct the collision as well as pin down the properties of the progenitor (e.g ??).

Before the Data Release 2 (?) of the ESA's Gaia mission (?), five large and diffuse cloud-like structures had been discovered in the Galaxy's halo. These include: the Virgo Over-Density (VOD, ?????), the Hercules-Aquila Cloud (HAC, ??), the Trinagulum-Andromeda structure (Tri-And, ???), the Pisces Over-density (???) and the Eridanus-Phoenix over-density (Eri-Pho, ?). According to the most recent investigations, Tri-And likely comprises of Galactic disc stars kicked out of the plane in a recent interaction with a dwarf galaxy, probably the Sagittarius dSph (e.g. ???). Of the remaining four, the Pisces overdensity clearly stands out as it reaches much larger Galacto-centric distances. On the other hand, the VOD, HAC and Eri-Pho structures occupy a very similar range of distances, between 10 and 20 kpc from the Galactic center. This lead ? to suggest that these three Clouds could all be part of one merger event, a galaxy accreted onto the Milky Way on a polar orbit (see also ?).

As demonstrated by the recent re-interpretation of the Monoceros Ring (and the associated sub-structures) and the Tri-And, deciphering the nature of halo over-densities is often impossible without either high-resolution spectroscopy (e.g. ?) or accurate astrometry (e.g. ??). In this Letter, we look for clues to the formation of the Hercules-Aquila and Virgo Clouds using proper motions provided as part of the Gaia DR2. At our disposal are highly pure samples of members of each Cloud, namely the RR Lyrae stars that i) are co-spatial with HAC and VOD in 3-D and ii) that have their line-of-sight velocities measured. By complementing the publicly available 4-D data with the GDR2 proper motions, we build a large tracer set with complete 6-D phase space information and study the make-up of each structure using the orbital properties of the constituent stars.

2 DATA AND ANALYSIS

2.1 4-D data

The Hercules-Aquila and Virgo Clouds are revealed unambiguously as overdensities of RR Lyrae in the halo, which peak at similar heliocentric distances, ∼17 kpc (HAC: ?) and ∼19 kpc (VOD: ???) respectively, but in opposite quadrants (e.g. their distribution in Galactic coordinates in Fig. 1). Other tracers (e.g. BHBs, MSTO, K giants) have been used to pin down the morphology of the Clouds with slightly inconsistent results between them, caused by poor distance determination, scarcity or simply trace the structures differently; therefore, the most recent kinematic follow-ups of the clouds have used RR Lyrae selected in the vicinity of the overdensities peak:

★ E-mail: mn@ras.org.uk (KTS)

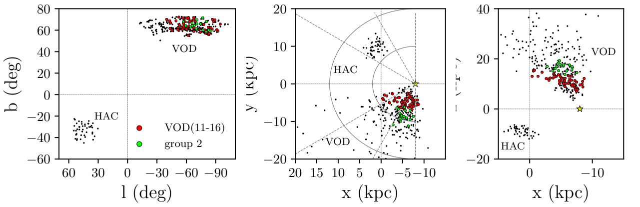

Figure 1. Spatial distribution of the RR Lyrae used in this work with full 6-D phase space measurements, in Galactic coordinates (left panel) and in the $x-y$ (middle) and $y-z$ (right) planes. The HAC field contains 44 RR Lyrae which likely belong to the Cloud with measured line-of-sight velocities (Simion et al. 2018) and Gaia DR2 proper motions. The VOD field contains 411 RRL which belong to several halo associations, including the Sagittarius stream and the VOD, with line-of-sight velocities provided by Vivas et al. 2016 and proper motions from Gaia DR2. In particular we mark group 2, a 'high significance' kinematical group, which contains 18 stars (green circles). The semi-circles are centred on the Sun's position and have radius of 10 and 20 kpc. The Sun (yellow star) is located at ($x_\odot$, $y_\odot$, $z_\odot$) = (0,-8,0) kpc and the Galactic centre at (0,0,0) - black circle.

- ? provide a table of 46 RRL with radial velocity measurements (45 observed with MDM and 1 from SDSS) with heliocentric distances between 15 and 18 kpc;
- ? compiled a catalog of 412 RRL in the region of the sky covered by the VOD with distances between 4 and 75 kpc from the Sun with radial velocity measurements from La Silla-QUEST, QUEST, CRTS and LINEAR.

2.2 6-D data: velocity distributions

From the two tables of RR Lyrae with 4D measurements, 44 stars in the HAC field and 411 in the VOD field have matches in GDR2 within 2" and proper motion measurements. The only star in the VOD region without proper motion belongs to a 'high-significance' kinematical group (group 1), likely the Sagittarius stream, identified by ?. This group contains 113 stars (112 with proper motions) which we remove from the VOD sample as a major contaminant of the field. The spatial distribution of the remaining stars (44 from ? and 299 from ?) with full 6-D phase space measurements is illustrated in Figure 1, in Galactic coordinates (left panel) and in the (x-y) Galactic plane and the (x-z) plane, perpendicular to (x-y). We adopted a left-handed Galactic Cartesian coordinates with the Sun located at ($x_\odot$,$y_\odot$, $z_\odot$) = (-8,0,0) kpc, the x-axis positive in the direction of the Galactic center, y-axis oriented along the Galactic rotation and the z-axis directed towards the north Galactic pole.

While ? identify 6 significant kinematical groups in the VOD field (their table 5) only groups 1 (Sagittarius stream) and 2 (likely members of the VOD, with $< v_{GSR} >$ = 135 km/s) contain more than 10 stars. We mark group 2 with green circles in Figure 1. We also mark with red circles the location of a group of stars with galactocentric distances similar to the HAC sample, 11< r_{GC}/kpc< 16 as we intend to follow their velocity distribution and orbital properties.

The velocity distribution in the VOD and HAC fields is shown in Fig. ?? in spherical polar coordinates, where v_r, v_θ, v_ϕ are the radial, azimuthal and polar components respectively. 'Group 2' stars (lime) form a group at v_r = 135 km/s as expected, while the stars at intermediate r_{GC} (red) seem to have a velocity distribution very similar to HAC, shown in the top panels. To estimate the error on each velocity component we resample the data 1000 times from a multivariate Gaussian distribution with mean the measurement $\{\alpha, \delta, d_{helio}, \mu_\alpha \cos(\delta), \mu_\delta, v_{helio}\}_i$ and full covariance matrix which takes into account the covariances between the right ascension α, declination δ and proper motions, provided by GDR2. We take the standard deviation of the resulting $\{v_r$, v_θ, $v_\phi\}$ distributions as the upper limit of the velocity uncertainties and show them in Fig. ??.

We calculate the velocity anisotropy in the two fields, keeping in mind the two samples span very different distance ranges. We compute the median and standard deviation over 500 non parametric bootstrap resampling trials, where each trial was modelled with a velocity ellipsoid using the Extreme Deconvolution module implemented in astroML (?). We find the HAC stars have radially biased orbits (β =

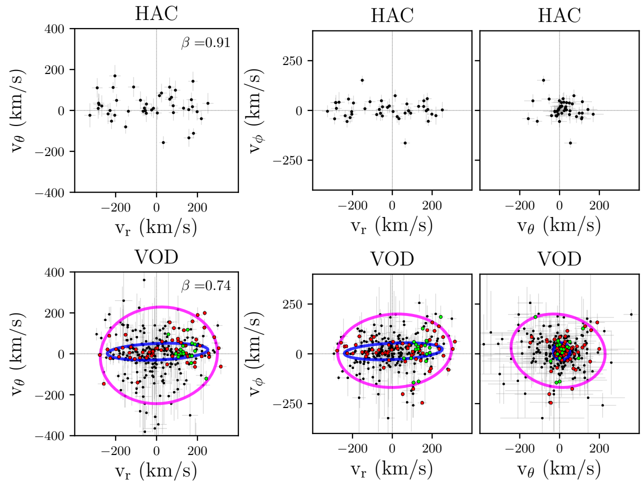

Figure 2. RRL velocity distribution in spherical polar coordinates (v_r, v_θ, v_ϕ are the radial, azimuthal and polar components respectively) in the HAC field (top row) and the VOD field (middle and bottom rows). The error on the velocity components of each star i, $[\sigma^i_{v_r}, \sigma^i_{v_\theta}, \sigma^i_{v_\phi}]$, has been propagated by randomly drawing 1000 stars from a multivariate Gaussian distribution with mean the measurement (ra^i, dec^i, d^i, $pmra^i$, $pmdec^i$, v^i_h) and full covariance matrix (takes into account the covariances between ra,dec and proper motions). The orbital anisotropy, is highly radial in the HAC field ($\beta = 0.91 \pm 0.03$) where the stars are most likely members of the Cloud and mildly radial in the VOD field ($\beta = 0.74 \pm 0.04$) in which stars span a much wider range of distances (see Fig. 1).

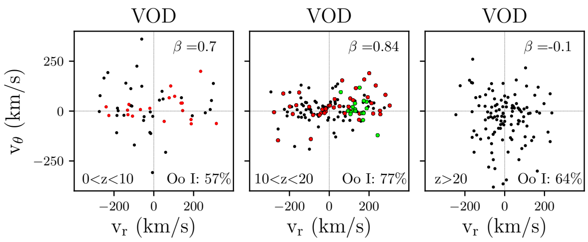

Figure 3. Radial versus azimuthal velocity in the VOD field, in three distance ranges above the Galactic plane. The fraction of RR Lyrae of Oosterhoff type I is reported in each panel.

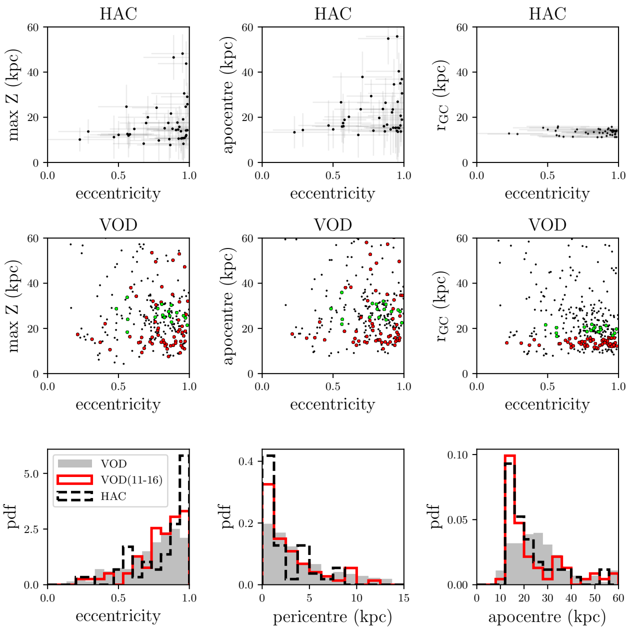

Figure 4. Orbital properties of the stars in the HAC and VOD fields. 'group 2' has similar orbital properties to the HAC, however it does not display a sausage velocity distribution (see middle row figure 2) - they are concentrated at $vr = 135$km/s as calculated by Vivas et al. 2016.

0.91 ± 0.03) while the VOD stars have slightly less radial orbits ($\beta = 0.74 \pm 0.04$).
We fit a model with two multivariate Gaussians to the VOD velocity ellipsoid using Extreme Deconvolution and obtain $\beta_1 = 0.96^{+0.02}_{-0.44}$ (marked in magenta in Fig. **??**) and $\beta_2 = 0.44^{+0.45}_{-0.20}$ (blue).

Fig. **??** shows the behaviour of the VOD azimuthal v_θ and radial v_r velocity distributions in 3 distanges ranges above the Galactic plane. In each slice we have calculated the fraction of Oosterhoff type I (Oo I) RR Lyrae, using equations 1 and 2 in **?** to classify the RRL into two types. According to this classification, Oosterhoff type II (Oo II) RR Lyrae will incude both Oo II and Intermediate objects. In the 10<z/kpc<20 range, where the velocity anisotropy is the highest ($\beta = 0.84 \pm 0.03$) approaching the value in the HAC field, the Oo I type dominates (77%). In the same slice, 73% of the stars belong to the more squashed (or 'sausage' looking) velocity ellipsoid. The same behaviour but less accentuated can be noticed in the 0<z/kpc<10 slice where the anisotropy $\beta = 0.7 \pm 0.1$ is lower but the fraction of Oo I stars decreases drammatically to 57%. Further from the plane, at z>20 kpc, the velocity ellipsoid is almost isotropic with $\beta = -0.1 \pm 0.2$. Here, the β value may still be affected by the presence of the Sagittarius stream in the field. Group 2 and red points are all located at $z < 20$ kpc, with the red points following an anisotropic velocity distribution.

2.3 Orbital properties of the HAC and VOD

For orbit integration we use the galpy package **?** in the recommended MWPotential2014 model for the Galactic potential which is composed of a Miyamoto-Nagai disc, a bulge with a power-law density profile that is exponentially cut-off, and a dark matter halo described by a NFW potential. The parameters are given in **?**, table 1. The resulting orbital parameters of the HAC and VOD are given in Fig **??**. To compute the errors (not shown for VOD to simply the figure) we integrated 500 orbits for each star where the orbits were initialised on parameters resampled from data, as in the previous section. The pdfs of the eccentricities, apocentres and pericentres are also shown. If the HAC orbits are clearly highly eccentric, we find that the majority of stars in VOD are also on quite eccentric orbits: in particular, the stars with $11 < r_{GC}$/kpc< 16 (in red), follow closely the HAC orbital properties.

3 ARE THE VOD AND THE HAC RELATED?

In this section we discuss the possible connection between the two clouds. We use the 6-D phase space measurements as initial conditions for backward orbit integration. We integrate the orbits for 8 Gyrs and show them in Fig. **??**.

4 CONCLUSIONS

Using a sample of ~500 RR Lyrae with full 6-D phase space information, we have studied the orbital properties of the Hercules-Aquila and Virgo Clouds. Both Clouds appear dominated by stars on highly eccentric orbits. Assuming that the kinematics of each structure is well described by a single Gaussian, the orbital anisotropy of the HAC is $\beta = 0.91$ and for the VOD, $\beta = 0.74$. Note, however that the original criteria applied to the RR Lyrae stars to select targets for spectroscopic follow-up differ drastically between the HAC and the VOD datasets. The HAC sample covers a very limited region in the of l, b, D space, while the VOD dataset spans a wide range of longitudes, latitudes and heliocentric distances. It is therefore likely that the VOD dataset contains a mixture of several halo sub-structures (see **?**, for a detailed discussion). For the entirety of the analysis described here, we made sure to cull the probable Sgr stream members. Additionally, we explore how the VOD's make-up changes with Galactic height and demonstrate that for $|z| < 20$ kpc, the VOD orbital anisotropy is $\beta \sim 0.84$, while above this threshold, it quickly changes to $\beta \sim 0$. We conclude therefore, that an assumption of a single Gaussian for the entire VOD sample is not appropriate. Modeling the kinematics of the VOD stars with a mixture of 2 multi-variate Gaussians, we show that two thirds of the VOD sample are the stars with $\beta = 0.96$, while the remainder has $\beta = 0.44$, in good agreement with the local measurement presented in **?**.

As revealed by Gaia, the two structures are composed of stars on nearly radial orbits, with peaks in the eccentricity distribution at 0.9 (0.8) for the HAC (VOD). The distributions of the peri-centric and apo-centric distances also match: the stars in the Clouds turn around at $1-3$ and $15-30$ kpc. Not only the HAC and the VOD look alike kinematically, their orbital composition is in perfect agreement with the stellar halo properties as analysed locally by **?** and globally (out to 40 kpc) by **?**. As these authors demonstrate, the inner halo is dominated by metal-rich debris from an old

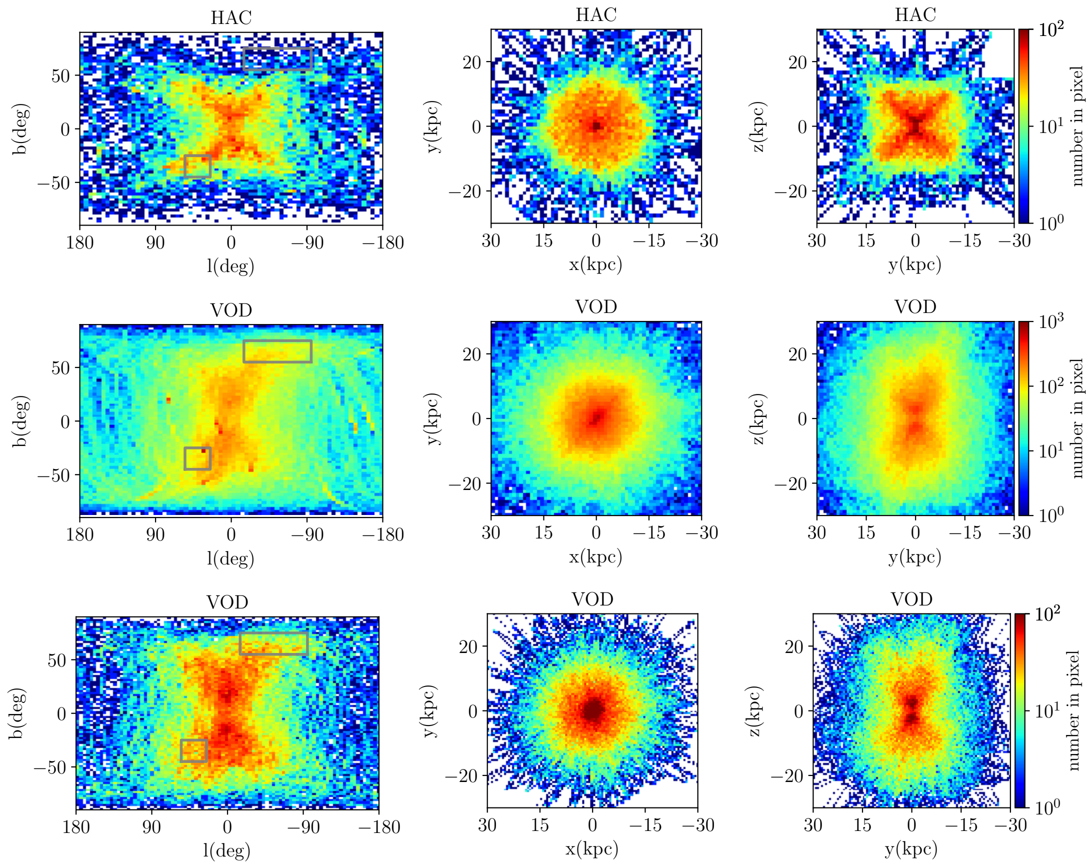

Figure 5. The backward orbit integration for HAC (top panels) and VOD (bottom panels) for 8 Gyrs look back time. We use $M_{vir} = 0.8 \times 10^{12} M_{\odot}$, the default galpy value . log(N) shown, notice the change in colour scale between top and bottom rows. The present day loci of HAC and VOD are marked with gray rectangles. The initial conditions of 44 stars with heliocentric distances between 15 and 18 kpc were used for the HAC backward orbit integration and of 299 stars with heliocentric distances between 4 and 75 kpc for the VOD orbit integration.

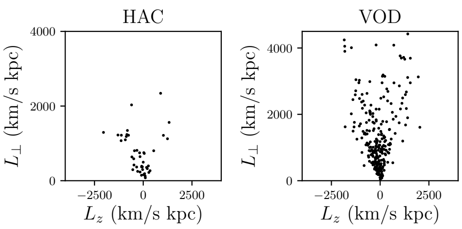

Figure 6. EXTRA: angular momentum - I can combine these two and also add another panel with energy vs total L when I figure out the energy.

and massive accretion event. In particular, **?** use Cosmological simulations of Milky Way halo formation, to bracket the time of the merger - between 8 and 11 Gyr ago - and its mass, which they show to be in excess of $10^{10} M_{\odot}$. The telltale sign of this dramatic head-on collision is the particular shape of the corresponding stellar velocity ellipsoid, which is stretched so much in the radial direction compared to the tangential ones, that it resembles a sausage. An alternative view of this merger can be found in **?**, where the local stellar halo is mapped out in the action space. Here, the metal-rich stars are shown have extended radial action distribution in addition to a prominent spray of material on retrograde orbits. The high mass of the progenitor is evidenced not only by the metallicity distribution of its likely member or the numerical simulations of halo formation, but also by a sizeable number of Globular Clusters that could be attributed to the same event (see **?**).

ACKNOWLEDGEMENTS

The Acknowledgements section is not numbered. Here you can thank helpful colleagues, acknowledge funding agencies, telescopes and facilities used etc. Try to keep it short.

REFERENCES

Amorisco N. C., 2015, MNRAS, 450, 575
Belokurov V., Deason A. J., Koposov S. E., Catelan M., Erkal D., Drake A. J., Evans N. W., 2018a, MNRAS, 477, 1472
Belokurov V., Erkal D., Evans N. W., Koposov S. E., Deason A. J., 2018b, MNRAS, 478, 611
Belokurov V., Evans N. W., Bell E. F., Irwin M. J. et al., 2007, ApJ, 657, L89
Bergemann M., Sesar B., Cohen J. G., Serenelli A. M. et al., 2018, Nature, 555, 334

Binney J., Tremaine S., 2008, Galactic Dynamics: Second Edition. Princeton University Press
Bonaca A., Jurić M., Ivezić Ž., Bizyaev D. et al., 2012, AJ, 143, 105
Bovy J., 2015, ApJS, 216, 29
de Boer T. J. L., Belokurov V., Koposov S. E., 2018, MNRAS, 473, 647
Deason A. J., Belokurov V., Evans N. W., 2011, MNRAS, 416, 2903
Deason A. J., Belokurov V., Evans N. W., Johnston K. V., 2013, ApJ, 763, 113
Deason A. J., Belokurov V., Hamren K. M., Koposov S. E. et al., 2014, MNRAS, 444, 3975
Deason A. J., Belokurov V., Koposov S. E., 2018a, MNRAS, 473, 2428
Deason A. J., Belokurov V., Koposov S. E., Lancaster L., 2018b, ArXiv e-prints
Duffau S., Vivas A. K., Zinn R., Méndez R. A., Ruiz M. T., 2014, A&A, 566, A118
Duffau S., Zinn R., Vivas A. K., Carraro G., Méndez R. A., Winnick R., Gallart C., 2006, ApJ, 636, L97
Gaia Collaboration, Brown A. G. A., Vallenari A., Prusti T., de Bruijne J. H. J., Babusiaux C., Bailer-Jones C. A. L., 2018, ArXiv e-prints
Gaia Collaboration, Prusti T., de Bruijne J. H. J., Brown A. G. A. et al., 2016, A&A, 595, A1
Hayes C. R., Majewski S. R., Hasselquist S., Beaton R. L. et al., 2018, ApJ, 859, L8
Hendel D., Johnston K. V., 2015, MNRAS, 454, 2472
Hildebrand A. R., Penfield G. T., Kring D. A., Pilkington M., Camargo Z. A., Jacobsen S. B., Boynton W. V., 1991, Geology, 19, 867
Johnston K. V., 2016, in Astrophysics and Space Science Library, Vol. 420, Tidal Streams in the Local Group and Beyond, Newberg H. J., Carlin J. L., eds., p. 141
Jurić M., Ivezić Ž., Brooks A., Lupton R. H. et al., 2008, ApJ, 673, 864
Li T. S., Balbinot E., Mondrik N., Marshall J. L. et al., 2016, ApJ, 817, 135
Majewski S. R., Ostheimer J. C., Rocha-Pinto H. J., Patterson R. J., Guhathakurta P., Reitzel D., 2004, ApJ, 615, 738
Morgan J. V., Gulick S. P. S., Bralower T., Chenot E. et al., 2016, Science, 354, 878
Myeong G. C., Evans N. W., Belokurov V., Sanders J. L., Koposov S. E., 2018a, ApJ, 856, L26
Myeong G. C., Evans N. W., Belokurov V., Sanders J. L., Koposov S. E., 2018b, ArXiv e-prints
Newberg H. J., Yanny B., Rockosi C., Grebel E. K. et al., 2002, ApJ, 569, 245
Nie J. D., Smith M. C., Belokurov V., Fan X. H. et al., 2015, ApJ, 810, 153
Price-Whelan A. M., Johnston K. V., Sheffield A. A., Laporte C. F. P., Sesar B., 2015, MNRAS, 452, 676
Rocha-Pinto H. J., Majewski S. R., Skrutskie M. F., Crane J. D., Patterson R. J., 2004, ApJ, 615, 732
Sanderson R. E., Helmi A., 2013, MNRAS, 435, 378
Sesar B., Ivezić Ž., Lupton R. H., Jurić M. et al., 2007, AJ, 134, 2236
Simion I. T., Belokurov V., Irwin M., Koposov S. E., 2014, MNRAS, 440, 161
Simion I. T., Belokurov V., Koposov S. E., Sheffield A., Johnston K. V., 2018, MNRAS, 476, 3913
Vanderplas J., Connolly A., Ivezić Ž., Gray A., 2012, in Conference on Intelligent Data Understanding (CIDU), pp. 47 –54
Vivas A. K., Zinn R., 2006, AJ, 132, 714
Vivas A. K., Zinn R., Andrews P., Bailyn C. et al., 2001, ApJ, 554, L33
Vivas A. K., Zinn R., Farmer J., Duffau S., Ping Y., 2016, ApJ, 831, 165
Watkins L. L., Evans N. W., Belokurov V., Smith M. C. et al., 2009, MNRAS, 398, 1757

This paper has been typeset from a TEX/LATEX file prepared by the author.